Noncontact Tremor Characterization Using Low-Power Wideband Radar Technology

Gaddi Blumrosen*, Moshe Uziel, Boris Rubinsky, and Dana Porrat

***Abstract*—Continuous monitoring and analysis of tremor is important for the diagnosis and establishment of treatments in many neurological disorders. This paper describes noncontact assessment of tremor characteristics obtained by an experimental new ultrawideband (UWB) system. The system is based on transmission of a wideband electromagnetic signal with extremely low power, and analysis of the received signal, which is composed of many propagation paths reflected from the patient and its surroundings. A description of the physical principles behind the technology, a criterion, and efficient algorithms to assess tremor characteristics from the bulk UWB measurements are given. A feasibility test for the technology was conducted using a UWB system prototype, an arm model that mimics tremor, and a reference video system. The set of UWB system frequencies and amplitudes estimations were highly correlated with the video system estimations with an average error in the scale of 0.1 Hz and 1 mm for the frequency and amplitude estimations, respectively. The new UWB-based system does not require attaching active markers or inertial sensors to the body, can give displacement information and kinematic features from multiple body parts, is not limited by the range captured by the optical lens, has high indoor volume coverage as it can penetrate through walls, and does not require calibration to obtain amplitude estimations.**

***Index Terms*—Body sensor, optics, Parkinson's disease (PD), tremor, ultrawideband (UWB).**

I. Introduction

TREMOR is the target symptom in the treatment of numerous neurological disorders such as Parkinson's disease (PD), midbrain tremor, and essential tremor.

These neurological disorder tremors vary in the conditions in which they occur and are categorized as rest, action, and postural tremors. PD is a growing problem affecting 120–180 victims out of every 100 000 people. While investigators have discovered many of the brain's mechanisms related to it (see, e.g., [1]), the causes of the disease are still unknown, and the clinical distinction can be difficult to identify. PD tremor has a typical frequency that ranges between 3 and 7 Hz, while other tremors can have a frequency above 10 Hz.

For clinical research purposes, a number of scales have been developed for a semiquantitative assessment of the frequency and magnitude of tremor. Unified Parkinson's Disease Rating Scale (UPDRS) scale is used for monitoring the PD disease progression and to indicate treatment effectiveness [2]. This scale is roughly estimated by the physician or nurse and is subjective. The experience of a nurse in a small clinic may be different from that of her colleague in a large clinic and they may give different scores for the same tremor. In addition, the UPDRS scale is composed only from 5 numbers since it is impossible to quantify delicate changes in the tremor.

An objective, reliable, and accurate tool for assessing disease severity and for home monitoring of PD patients has significant importance for diagnosis and establishment of treatments [3]. Decades of research have produced several objective instrumental approaches for the assessment of tremor [4] which include inertial sensors (INS) [5]–[9] optical tracking systems [10]–[14] tracking devices that exploit electromagnetic (EM) radiation properties like [15]–[20]. These technologies are objective and can be compared and integrated with subjective scores.

INS such as accelerometers [6] or gyroscopes [7] are popular for tremor assessment. They can give information about the tremor amplitude and frequency [6]. An INS must be attached to specific patient's body parts. It can continuously measure tremor during daily life activities, e.g., by an actigraph in a wrist-watch-like package [5]. The tremor frequency estimation error obtained by an accelerometer is less than 0.5 Hz [19]. The amplitude estimation error depends on the tremor pattern, the algorithm used, and the specific hardware, and is usually on scale of a millimeter [20]. In many cases, wearing the INS is not comfortable, its battery has to be replaced every day, it can provide information only about limited number of body parts [21], and in some cases, the tremor amplitude accuracy is affected by accelerometer and gyroscope drifts [7], [8] and by the effect of the gravity in acceleration measurements [9].

Optical technology can also be used for tremor tracking. It is usually implemented by a video recording system and is commonly used in gait analysis laboratories [10]. Tremor is usually assessed by attaching a lightweight marker with known color and intensity attributes to the tremulous body part (TBP) of interest and extracting, by signal-processing techniques, the pixels per each video frame that belong to the TBP [12]. For tracking body parts displacements, a precise offline calibration

Manuscript received August 11, 2011; revised October 26, 2011 and November 16, 2011; accepted November 20, 2011. Date of publication December 2, 2011; date of current version February 17, 2012. *Asterisk indicates corresponding author.*

*G. Blumrosen was with the School of Computer Science and Engineering, Hebrew University of Jerusalem, Jerusalem 91904, Israel. He is now with Tel Aviv University, Tel Aviv 69978, Israel (e-mail: gaddi.b@gmail.com).

M. Uziel was with the School of Computer Science and Engineering, Hebrew University of Jerusalem, Jerusalem 91904, Israel. He is now with Insightec Ltd., Tirat Carmel, 39120 Israel (e-mail: uzikiko@gmail.com).

B. Rubinsky is with the Graduate Program in Biophysics and Department of Mechanical Engineering, University of California at Berkeley, Berkeley, CA 94720 USA (e-mail: rubinsky@me.berkeley.edu).

D. Porrat is with the School of Computer Science and Engineering, Hebrew University of Jerusalem, Jerusalem 91904, Israel (e-mail: dana.porrat@huji.ac.il).

Color versions of one or more of the figures in this paper are available online at http://ieeexplore.ieee.org.

Digital Object Identifier 10.1109/TBME.2011.2177977

is needed [13]. The tremor frequency estimation obtained by an ordinary video based system is around 0.1 Hz [14]. The amplitude estimation error ranges from less than 1 mm to a few centimeters and depends on the environment setting and the camera quality. The estimation error decreases with the frame rate and with the number of pixels representing the marker in the frame. A markerless video system that uses an advanced segmentation technique on the different body parts was used in [22] for tracking of hand articulations. Markerless techniques are not as accurate as ones with a marker [4] and the displacement estimation resolution decreases with the distance between the camera and the patient. As a result, markerless video systems might not be suitable to give the tracking accuracy needed for characterizing tremor. Since the video system restricts patient location to the range captured by the video camera, it cannot be used for continuous assessment of tremor during daily life activities.

EM-based devices are also used in tremor assessment. For instance, Nizet *et al*. [17] use a commercial pen-shaped laser pointer for assessment of upper limb tremors. This assessment is less accurate than video or motion detection devices and is limited to arm and hand tremor. Padraig and Richard [18] used a magnetic tracking device that analyzes changes in the magnetic field observed by a sensor attached to the patient's body. The system has poor performance when the patient is farther than 1 m from the device. Ivan [15] uses direct recording of the electrical activity produced by skeletal muscles using electromyographic systems, but requires electrical contact with the patient and is very sensitive to displacement of the sensor.

A narrow-band radar has been used [23] for the detection and classification of patients' movements and location based on the Doppler effect. When humans walk, the motion of various components of the body including the torso, arms, and legs produce a characteristic Doppler signature. Fourier transform techniques were used in [23] to analyze these signatures and identify key features representative of the human walking motion. Short-time Fourier transform can be applied using a sliding window on the temporal signal to produce a spectrogram of human radar signature that describes human motion in the frequency and time domains. High frequencies in the spectrogram are related to high Doppler shifts which correspond to fast body movement, usually of arms and feet. Gurbtiz *et al*. [24] derive maximum likelihood estimators to obtain the average displacement of different body parts from the spectrogram. Hornsteiner and Detlefsen [25] use a classifier on the human body radar signature to characterize gait, in particular, step rate and mean velocity. Motion kinematics, like walking speed and gait variability, can be used to assess severity of PD [26]. Radar techniques based on low frequencies content (less than 1 GHz) are not used to detect tremor because of their low temporal and spatial resolution of around few centimeters [27], which is not adequate for detection of typical tremors.

Ultrawideband (UWB) radio is a technology that uses a large portion of the radio spectrum. It can be used with very low energy levels for short-range high-bandwidth communications. The potential value of the UWB radio technique stems from its use of extremely wide transmission bandwidths. It yields accurate position location, lack of significant fading, and possible material penetration [28]. A wireless sensor network (WSN) based on a UWB radio Physical layer (PHY) is specified in IEEE 802.15.4a [29]. A UWB-based WSN can be used at the same time as a wireless body sensor network as a system for range and location estimation [30]. UWB-based radar has been suggested for use for medical applications in [31]. Chang and Sahai [32] describe tracking a human with a 2-D UWB sensor network. Zhuge *et al*. [33] suggest using UWB radar to image a human body. Staderini *et al*. [34] suggests the use of UWB radar for cardiac biomechanic assessment and chest movement assessment, obstructive sleep apnea, and sudden infact death syndrome monitoring. Lavitas *et al*. [35] show results in a scale of a centimeter for detection of personal respiratory movements and heart beating of several patients. Mahfouz *et al*. [16] use an active UWB tag for surgical navigation and achieves a mean estimation error of 5 mm.

In an earlier study [36], we suggested the use of UWB radar technology for assessing and quantifying tremor. That paper describes the basic technology and gives some preliminary results. In a followup study [37], we suggested using a UWB-based WSN equipped with at least three sensor nodes for assessment of tremor in three dimensions. In this paper, we broaden the work in [36] and [37], examine aspects that will make this technology suitable for future clinical usage, and compare to other common technologies to assess tremor. For a feasibility test, a UWB tremor acquisition system prototype was used for capturing a tremor of an arm model. A series of experiments was conducted with induced tremor frequencies in the range of clinical tremor frequencies. The system was tested with different distances between the UWB acquisition system and the arm, and with different interferers, to simulate real conditions. The estimated frequencies were similar to the induced frequencies with an estimation error of less than 0.1 Hz. The set of estimated frequencies were compared to those obtained by a standard video recording system and have shown to be highly correlated with an estimation error in the scale of a millimeter.

The UWB-based tremor acquisition technology suggested in this study promises to give n uniform objective scale of the severity of many neurological diseases that relate to tremor. With this technology, small changes in the tremor that cannot be determined by the physician in the clinics can be detected continuously during daily life activities and facilitate faster monitoring and treatment. Using the UWB-based technology will allow monitoring continuously the effect of a treatment and save suffering from those who do not respond well to it. Furthermore, this method can be used as feedback to drug delivery mechanisms for PD patients and to tune in real-time deep brain stimulation parameters.

This study differs from other UWB technologies in four main aspects. First, it suggests for the time to estimate tremor parameters through UWB measurements. For this purpose, efficient analytical methods with low complexity were derived. Unlike common techniques, that try to estimate the absolute displacement, the analytical methods in this study estimate only the relative displacements of the body part relative to its gross movement. Second, it uses *a priori* clinical constraints about

the tremor frequencies and amplitudes range that are used to filter out undesired components of the signal. Third, this study suggests using a common UWB-based location algorithm that first locate the patient and then to filter out the signal reflections that are not from around the patient. By this, large portion of the undesired signal is excluded, and the data analysis complexity is further reduced. Fourth, unlike common tracking methods that are based on UWB tags and are limited to certain body part, this study suggests to use all of the reflections from the body. As a result, this method can be used to assess tremor characteristics from the all body.

The UWB-based technology has major advantages over existing technologies that try to give an objective scale for the tremor. It is not wearable like INS sensors; it can include information from all body parts and also information about patient motion kinematic and it is not restricted to light conditions or to narrow location as in optical systems.

This paper is organized as follows. Section II describes a physical model of tremor. Section III includes a statistical criterion and efficient algorithms to assess tremor characteristics. Section IV describes the experimental setup for evaluation of the UWB system in different conditions. In Section V, the experimental results are given and discussed. A comparison of the UWB system and other different tremor acquisition system is given. Section VI summarizes the results and suggests directions for future research.

II. System Model

A. Patient Tremor Modeling

Human movement is composed of slow dynamics (e.g., gait cycle) and fast dynamics (e.g., tremor) components. Each body part displacement in time has a different associated pattern [25]. The displacement of the entire body due to tremor can be described by the displacement of each of its TBPs. We will separate the body to L TBPs, indexed by l, $l = 1, \ldots, L$. Each lth TBP is well distinguished by its location and sometimes by its temporal tremor characteristics. We model the displacement of the lth body part in a Cartesian coordinate axis in reference to the acquisition system location at instance time t by

$$\boldsymbol{b}_l(t) = \boldsymbol{b}_{l,s}(t) + \boldsymbol{b}_{l,g}(t) + \boldsymbol{b}_{l,f}(t) \tag{1}$$

where $\boldsymbol{b}_{l,s}(t)$ is the lth TBP's absolute displacement component of very slow movements at instance time t, $(x_{l,s}(t), y_{l,s}(t), z_{l,s}(t))$, which reflects relatively static displacements, usually with frequency content of less than 0.5 Hz, e.g., torso movement; $b_{l,g}$ is the lth TBP's absolute displacement component of slow dynamics at instance time t, $(x_{l,g}(t), y_{l,g}(t), z_{l,g}(t))$, with frequency content in range of 0.5–2 Hz, and is related to daily life normal activities [38], e.g., gait, or respiration and articulation; $b_{l,f}$ is the lth TBP's absolute displacement component of fast dynamics at instance time t, $(x_{l,f}(t), y_{l,f}(t), z_{l,f}(t))$, having displacement fluctuation frequency in the range of 2–12 Hz, and is related to rapid displacement in abnormal activities like sport and tremor.

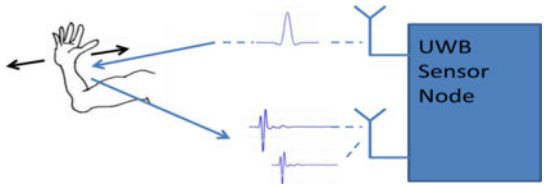

Fig. 1. UWB sensor node. It can assess motion in 1-D. The transmitted UWB pulse is reflected from the moving body part. The reflections of the signal are then analyzed and the characteristics of the tremor can be obtained. To assess tremor in 3-D, at least three UWB senor nodes employed in different locations are needed.

B. UWB-Based Tremor Acquisition System Model

The UWB system is composed of multiple sensor nodes with UWB radar capabilities. Each sensor node is equipped with a UWB transmitter, a receiver, a processing unit, and a storage unit. A UWB pulse is transmitted into the medium where the patient is located from each sensor node. The UWB sensor node receives reflections of the transmitted pulse from the medium. Each sensor node is capable of sensing tremor and motion features in 1-D. To assess tremor in 3-D, at least three senor nodes employed in different locations are needed. In this paper, the system model for one sensor node is described. Expansion to multiple nodes, with three well-synchronized sensors nodes, is given in [37]. Fig. 1 demonstrates a tracking device of an arm movement using a 1-D single UWB sensor node.

The signal that has propagated through a wireless channel consists of multiple replicas (echoes, mainly caused by reflections from objects in the medium) of the originally transmitted signal, named multipath components (MPCs). Each MPC is characterized by an attenuation and a delay [39]. The received signal at time instance t is

$$r(t) = \Sigma_{m,k}\beta_{m,k}(t-mT)p(t-mT-\tau_{m,k}) + n(t) \tag{2}$$

where $p(t)$ is a transmitted pulse with typical duration around 10 ns, m is the pulse index, T is the pulse repetition time, $\tau_{m,k}$ is the kth MPC delay in the mth pulse, $\beta_{m,k}$ is its related attenuation factor which is assumed constant during the observation time, and $n(t)$ is an additive noise component. The noise includes thermal and amplifier noise which can be modeled by white Gaussian processes, distortion from nonlinearity of the amplifiers, and interference of other radio signals from narrow band systems. The received signal is composed of desired MPCs reflected from TBPs, nondesired MPCs from other reflectors in the medium, and noise.

Each object in the environment reflects the signal with amplitude determined by the object reflection coefficient. The reflection coefficient of a TBP is determined by its tissue composition, by its cloth material, and by the signal frequency and bandwidth. Metal object reflect most of the radiation, i.e., have a reflection coefficient of nearly 1 [40]. Most of the reflection from the TBP is due to the relatively high conductivity of the blood and muscles which have nearly the impedance of water. At a signal frequency of 5 GHz, about 10% of the transmitted power is reflected back just from the heart muscle; the reflection from the all body can be more than 50% [41].

The received signal in (2) is sampled every period of T_s s. The samples of M consecutive pulse repetitions are stored in an observation matrix $\boldsymbol{r}$ of size $M \times N_h$, where $N_h = T/T_s$ is the number of samples in each pulse repetition. The matrix is given by

$$\boldsymbol{r} = \begin{pmatrix} \boldsymbol{r_1} \\ \vdots \\ \boldsymbol{r_m} \\ \vdots \\ \boldsymbol{r_M} \end{pmatrix} = \begin{pmatrix} r(t)|_{t=0,T_s \cdots (N_h-1)T_s} \\ \vdots \\ r(t)|_{t=(m-1)N_h T_s,(m-1)N_h+1)T_s \cdots (mN_h-1)T_s} \\ \vdots \\ r(t)|_{t=N_h M T_s,(N_h M+1)T_s \cdots (N_h M-1)T_s} \end{pmatrix} \tag{3}$$

where m, $1 \leq m \leq M$, is the pulse index.

The column dimension of $\boldsymbol{r}$ includes the received signal samples captured in the different pulse repetitions and, therefore, is related to time dimension. A row of $\boldsymbol{r}$ includes the received signal samples which are related to different MPCs of one transmitted pulse. These MPCs are related to different reflection of the pulse at different locations in the medium and, therefore, are related to spatial dimension. The distance between the reflecting object and the acquisition system is proportional to the MPC's delay and the propagation velocity which is equal to the speed of light. The spatial resolution in the observation matrix is proportional to the sampling period T_s and can be improved by utilizing the spatial-temporal correlation of the samples.

The pulse repetition period include signal reflections from all over the medium. To derive the tremor characteristics, our processing method first detects the MPC delays related to the TBP from the patient's nearby surrounding. A UWB-based localization algorithm, like the one in [32], can be utilized to reduce the observation matrix to a time interval that includes mainly the reflections from nearby the patient. The delays of all the MPCs related to the TBP can then be processed to give the TBP's frequency and amplitude.

III. Data Analysis

The data analysis is performed on the UWB received signal and is aimed to quantify the tremor from the samples stored in the observation matrix. The analysis is applied for one sensor node in single axis which is defined as the x-axis. An extension to 3-D with multiple sensors is given in [37].

First, a general nonlinear minimum mean square error (MMSE) criterion is presented to derive the TBP's absolute displacements out of the measurements. Then, we simplify the criterion to a linear one that tries to estimate the tremor displacements relative to the mean body part location. We describe the optimal solution to the criterion which is cumbersome for implementation and present an efficient suboptimal solution.

A. MMSE Criterion to Obtain TBP's Absolute Displacements

Tremor characteristics can be obtained by analyzing the absolute displacements of the TBP over time. The MMSE criterion for a transformation that extracts the lth TBP's displacement in 1-D from the received signal in (3) is

$$\hat{f} = \arg\min_{f} E\left\{ \left(f(\boldsymbol{r_m}) - \boldsymbol{b_{l,f}}(m) \right)^2 \right\} \tag{4}$$

where $\boldsymbol{b}_{l,f}(m)$ is the displacement at time index m of the lth TBP in the x-direction, $f(\cdot)$ is a transformation of the sampled received signal to displacement, $\boldsymbol{r_m}$ is an N_h length vector of received signal as defined in (3), and $E[\cdot]$ denotes expectation over all stochastic noise sources in the observation period.

Since the problem is not linear and not convex [42], the criterion in (4) can be solved only numerically. An optimal transformation requires accurate statistical knowledge [43] which is usually not available. Furthermore, the channel is commonly not stationary since the patient and other objects in the medium move during the observation period. As a result, a frequent update of the transformation is needed for an accurate approximation of the TBP's displacement and a feasible solution is cumbersome.

B. Linear MMSE Criterion to Obtain TBP's Relative Displacements

To try to simplify the solution of the problem, we simplify the criterion in (4). To distinguish between voluntary and undesired components, we can suggest estimating the TBP's displacement relative to the slow varying body part displacements instead of the absolute TBP's displacement in (4). The relative displacements of the TBP in relation to the TBP's slow varying displacements in the direction of the x-axis can be obtained from (1) and is given by

$$\boldsymbol{d_{l,f}}(m) = \boldsymbol{x_{l,f}}(m) - (\boldsymbol{x_{l,s}}(m) + \boldsymbol{x_{l,g}}(m)). \tag{5}$$

In a small observation period, the MPCs related to the TBP differ in time mainly by a time shift. This time shift is in a range that is determined by the tremor amplitude, and the frequency of the change of the time shifts in the observation period is determined by the tremor frequency. Therefore, by approximating the time shifts of MPCs reflected from the TBP, we can derive the relative TBP displacements and the tremor frequency and amplitude.

To further simplify the criterion in (4), we derive a new MMSE criterion for the relative TBPs' delay estimation in the observation period. The relative displacements are obtained by multiplying the delays by the speed of light. The general transformation $f(\cdot)$ is replaced by a linear transformation on the sampled received signal. The new criterion utilizes the statistical information from all pulse repetitions in the observation period and the known clinical tremor amplitude and frequency range. The new linear MMSE criterion is

$$\{\hat{\mathbf{w}}, \hat{\boldsymbol{\tau}}\} = \arg\min_{\mathbf{w},\boldsymbol{\tau}} E\left\{ \sum\nolimits_{m=1}^{m=M} \left(\mathbf{w}_{\tau_\mathbf{m}}^{\mathbf{T}} \mathbf{r}_\mathbf{m} - s_{l,m} \right)^2 \right\} \tag{6}$$

s.t.

$$\boldsymbol{w}_{\boldsymbol{\tau_m}}^{\boldsymbol{T}} \boldsymbol{w}_{\boldsymbol{\tau_m}} = 1$$

$$-\frac{A_t}{2c} < \tau_m < \frac{A_t}{2c}$$

$$f_{t_L} < \arg\max_{f} |\mathrm{FFT}(\boldsymbol{\tau})| < f_{t_H}$$

where r_m is an N_h length vector of the sampled received signal for pulse index m, $1 \leq m \leq M$, s_l is a scalar representing the signal energy reflected from the lth TBP surface for pulse index m, τ_m is the mth time shift which relates to the relative TBP displacement, $\boldsymbol{d_{l,f}}(m) = c\tau_m$, w_{τ_m} is an N_h length weight vector $\boldsymbol{w}$ shifted by τ_m, $w_{\tau_m}(n) = w(n - \tau_m)$, $\boldsymbol{\tau}$ is an M long vector that includes the TBP's relative time shifts, $\tau = \{\tau_1, \tau_2 \ldots \tau_M\}$, f_{t_L} and f_{t_H} are the lower and upper clinical tremor boundaries (usually 2–12 Hz), A_t is the maximal clinical tremor displacement (in the range 1–4 cm), and $E[\cdot]$ is the expectation operator in the observation period $w_{\tau_m}(n) = w(n - \tau_m)$.

The first constraint in (6) is the power constraint. The second constraint operates on observation matrix rows and limits the solution to the clinical tremor amplitude range; it is a spatial constraint. The third constraint operates on observation matrix columns and limits the solution to changes in the range of clinical tremor frequencies, and is a temporal constraint. Other constraints that reflect clinical properties of the tremor, i.e., displacement velocity or acceleration, can also be added.

C. Optimal Solution

An optimal solution to (6) is based on match filtering of the received signal and combining the result with the optimal MMSE weights [43]. A solution derived by methods of nonlinear programming [44] is cumbersome and its quality depends on the statistical parameters which are sometimes not available *a priori*, and their real-time estimations are accurate in nonstationary conditions.

D. Efficient Solution

A feasible solution to (6) is to first approximate the time shifts and then apply the constraints one after another to the result. The delays are proportional to the relative displacement of the TBP with the factor of the speed of light. From the relative displacement, the tremor frequency and amplitude and the medical diagnosis can be obtained. Fig. 2 describes the data analysis stages for the solution. The solution stages are the following.

1) MPCs Detection and Spatial Filtering: A peak detector can be used to detect the MPCs either on the match filtered output or directly on the samples [28]. A pulse detector can be implemented by using the Central Mass (CM) of the signal in a narrow window [45]. As a result, an approximation of the CM of the ith time shift of the mth pulse can be obtained by the received signal CM in the window W_s:

$$\dot{\boldsymbol{\tau}}_{\boldsymbol{m}}(i) = \frac{\sum_{i<n<w_s+i} \boldsymbol{r_m}(n) i}{\sum_{i<n<w_s+i} \boldsymbol{r_m}(n)} \tag{7}$$

where W_s is the sliding window length in samples in a range that includes typical tremor amplitudes and the UWB pulse shape period; the window index i moves from 1 to N_h.

This delay detection is computationally more efficient than the match filtering operation and is robust to pulse distortion in the window boundary. In addition, the sliding window operation is a spatial filtering operation since it excludes from the result undesired interferers that are not related to the tremor due to the window size in the range of a tremor.

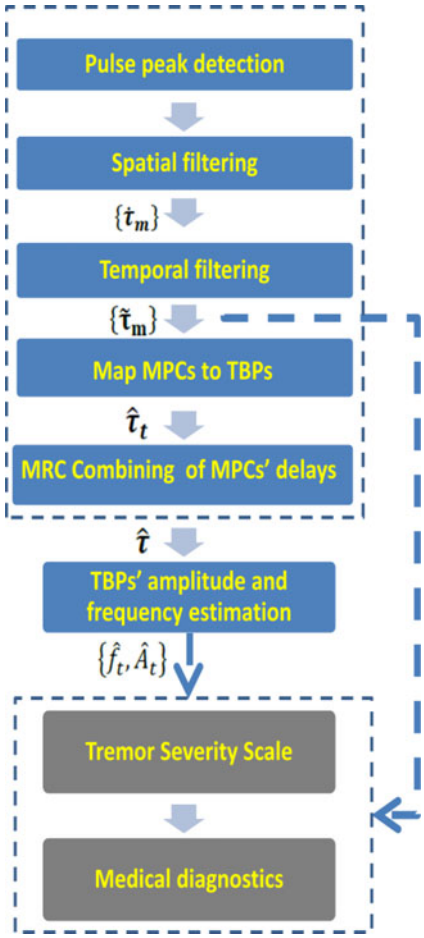

Fig. 2. Scheme that describes the data analysis stages. The tremor severity scale can be determined on either the tremor amplitude and frequency estimations of the specific TBP or directly on the filtered delays that capture information from all body parts.

2) Temporal Filtering: To exclude from the time shift approximations in (7), the effect of MPCs which are not related to the TBP like the ones reflected from static objects or from daily life movement of the torso, we apply the temporal constraint in (6). The temporal constraint results in a bandpass filter with a passband corresponding to the tremor frequency range. The ith filtered time shift vector is given by

$$(\tilde{\boldsymbol{\tau}}_{\mathbf{1}}(i)\tilde{\boldsymbol{\tau}}_{\mathbf{2}}(i) \ldots \tilde{\boldsymbol{\tau}}_{\boldsymbol{M}}(i) = (\dot{\boldsymbol{\tau}}_{\mathbf{1}}(i)\dot{\boldsymbol{\tau}}_{\mathbf{2}}(i) \ldots \dot{\boldsymbol{\tau}}_{\boldsymbol{M}}(i) * h_{\mathrm{BP}} \tag{8}$$

where $*$ is the convolution operation and h_{BP} is a N_h length vector with bandpass filter coefficients.

3) Mapping the MPCs to the TBP: A finger selection algorithm can be applied on the approximated time shifts to compute the set of dominant time shifts that are related to reflection from a single TBP and not to other reflections from other body parts or objects in the environment. A common finger selection mechanism is based on the received signal-to-noise ratio (SNR) [46].

The SNR of the *i*th time shift vector in (8) is calculated as

$$\mathrm{SNR}_i = \frac{\sum_{j=1, j\in P}^{j=M} \boldsymbol{F_i^2}(j)}{\sum_{j=1, j\notin P}^{j=M} \boldsymbol{F_i^2}(j)} \tag{9}$$

where $\boldsymbol{F}_i$ is the *M* length vector of absolute value of the Fourier Transpose of the filtered weight time shifts, $\boldsymbol{F_i} = |\mathrm{FFT}(\tilde{\boldsymbol{\tau}}_{\boldsymbol{i}})|$, and *P* is a set of dominant amplitude indices in the spectrum which can be determined by thresholding F_j.

Fingers are chosen by applying a threshold on the SNRs:

$$i \in K, \quad \text{if } (\mathrm{SNR}_i \geq \mathrm{SNR}_{\mathrm{TH}}) \tag{10}$$

where *K* is the group of selected fingers with size smaller than N_h, and $\mathrm{SNR}_{\mathrm{TH}}$ is the SNR threshold and can be fixed to a ratio of the maximal SNR's value, e.g., $\mathrm{SNR}_{\mathrm{TH}} = 0.8 \max\{\mathrm{SNR}_i\}$. More advanced finger selection algorithms, e.g., finger selection that maximize the signal interference and noise ratio (SINR), can be applied in the future.

4) Maximal Ratio Combining Combing of the MPCs: Maximal ratio combining (MRC) chooses MPCs with the highest SNRs and coincides with the MMSE optimal solution if MPCs are well separated and the noise is white [46] since overlapping MPCs distort each other. The *m*th time shift approximation after MRC combining is

$$\hat{\tau}_m = \sum_{i=1}^{S} \hat{\boldsymbol{w}}(i)\tilde{\boldsymbol{\tau}}_{\boldsymbol{m}}(i) \tag{11}$$

where the set of combining weights are MRC weights, $\hat{\boldsymbol{w}}(i) = \mathrm{SNR}_i$, the *i*th time shift SNR.

Unlike the MMSE combining, the MRC combining excludes the need of true channel statistics and furthermore is a numerically efficient way that strikes a balance between optimality and computational tractability.

E. Extracting Tremor Frequency and Amplitude

The set of tremor frequencies and amplitudes can be derived directly from the Fourier transform of the approximated time shift vector $\hat{\boldsymbol{\tau}}_{\boldsymbol{t}} = (\hat{\tau}_1, \hat{\tau}_2 \ldots \hat{\tau}_m \ldots \hat{\tau}_M)$. For a common case of one dominant tremor frequency, the tremor frequency estimation is

$$\hat{f}_t = \arg\max_f |\mathrm{FFT}(\hat{\boldsymbol{\tau}}_{\boldsymbol{t}})|. \tag{12}$$

The TBP can include several tremor amplitudes reflected from different locations along its surface. The maximal tremor amplitude is

$$\hat{A}_t = 2c\{\max|\mathrm{FFT}(\hat{\boldsymbol{\tau}}_{\boldsymbol{t}})|\}. \tag{13}$$

The solution in (12) and (13) can be extended to give 3-D relative displacement by using three or more sensor nodes as described in [37].

F. Extension of the Solution to Multiple TBPs

To extend the solution to multiple TBPs, there is a need to map the delays to the different TBPs. One common way in radar processing is to construct from Time of Arrival (ToA) an image of the patient [33]. MPCs with close ToA (MPCs' delays) are more likely to be related to the same TBP. This mapping becomes less accurate in a medium rich with scatterers that have no direct paths.

Another way to map MPCs to TBPs is to include the MPCs pattern of variation over time in the mapping. Similar reflection patterns indicate that it is more likely that MPCs are related to the same TBP. The mapping can exploit the fact that the reflection pattern varies in each body part as a function of the biological content of the body part tissue and its nature of movement, e.g., UWB MPCs reflected from the torso, which is relatively static, have different reflection pattern and set of amplitudes than the one from the arm.

Another way to map MPCs to TBPs is by wearing on the TBP of interest a cloth or a special sleeve with significantly different reflection characteristics from the other body parts. This will enable in the data analysis to distinguish between the delays of the TBP of interest and other body parts. For example, attaching a metal marker to the TBP of interest will magnify the reflections of the TBP compared to other body parts due to the higher reflection coefficient.

G. Medical Diagnostic

For medical diagnostics needed for disease classification and for treatment, an objective scale of tremor severity should be obtained. While tremor frequency content of different TBPs is often similar [1], tremor amplitudes content can vary for each TBP and, in some cases, can also include a set of tremor amplitudes reflected from different areas along the TBP.

The tremor severity scale can be either based on the tremor frequencies, on the entire set of amplitudes reflected from the TBP, on the average or the maximal tremor amplitude like in (14), or sometimes on the entire histogram of tremor frequencies or amplitudes from all TBPs of the patient, or even on the estimated MPC delays as shown in Fig. 2.

In case that the tremor severity scale is based on the histogram of amplitudes or delays, there is no need to map the delays to the different TBPs. The scale will include information from all body parts.

IV. Experimental Setup

The experimental setup consisted of a UWB 1-D tremor acquisition system composed of one sensor node prototype, a reference video recording system, and a tremulous arm model that mimicked a tremor. The arm model trembled with a frequency in the range of 3–12 Hz induced by a sine wave formed by a function generator (HP 3325A) and with amplitudes that varied from 0.3 mm to 3 cm. The induced frequency accuracy of the ac generator was 10 μHz. Both systems (UWB and video) were activated simultaneously and tried to capture tremor frequency and amplitude.

The UWB tremor acquisition system prototype consisted of a transmitter, a receiver, a storage unit, and a processing unit and. The UWB pulse was transmitted every pulse repetition from the transmitter antenna. The signal was received by the received

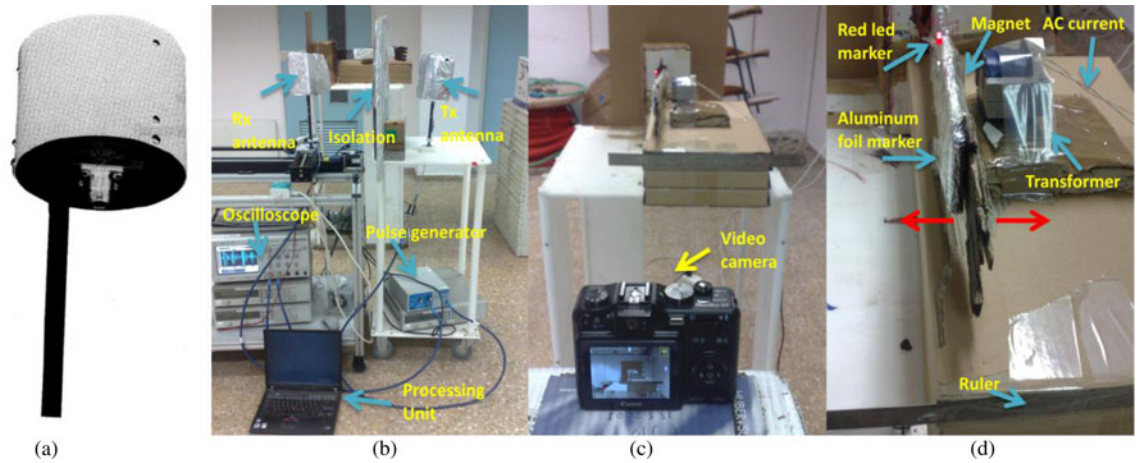

Fig. 3. Tremulous arm model and UWB and video tremor acquisition systems. (a) Omnidirectional antenna used for the UWB signal transmission and reception. (b) UWB tremor acquisition system was implemented with a UWB sensor node prototype that consists of a transmitter (pulse generator and Tx antenna), a receiver (Oscilloscope and Rx antenna) a processing unit, and a storage unit (notebook computers). (c) Video recording system consisted of a camera (Canon, G7) and computer for processing the raw data. (d) Tremulous arm was based on an electrical current which induced EM force that moved the arm in a cycle with a frequency of the ac current source. The arm surface was moving to and from the UWB acquisition system so the reflection surface was maximized and horizontal with respect to the video camera to capture full tremor amplitude.

antenna, processed, and then stored for analysis. Fig. 3(b) shows the UWB system prototype.

The transmitter was based on pulse generator (Picosecond Pulse Labs 4015D). The Pulse had a shape of a third derivation of a Gaussian with width of 100 ps (10-GHz bandwidth), and amplitude of 1.35 V. The repetition frequency was 85 Hz and the bandwidth was 8 GHz. The transmitted pulse was amplified by a 30-dB amplifier (AF2 1828A, Herotek) and then connected to an omnidirectional antenna. The transmission power was extremely low with peak power of 52 mW/cm^2, and an average power of 105 μW/cm^2, both measured at a distance of 1 m from the antenna.

The transmit (Tx) and receive (Rx) antennas were both implemented by same omnidirectional antennas (EM-6865, Electoro-Metrix). The antenna was capable of operating as either a transmitting or receiving antenna over the 2–18 GHz frequency range. It consisted of two brass conical elements connected point-to-point to form an hourglass-shaped antenna element. A 25.4-cm (10") support rod provided a means for mounting the antenna. The antenna is shown in Fig. 3(a). A metal cover structure was added over both transmit and receive antennas to enhance antenna gain and improve directionality. The antennas were isolated by a cardboard wrapped by aluminum foil to avoid a direct path.

The UWB signal was received by the received antenna. The receiver was based on an oscilloscope (DSO81304A, Agilent) with a sampling rate of 20 GS/s. The receiver was synchronized to the transmitter by a trigger from the pulse generator. The raw data were sent the oscilloscope memory for storage. The processing unit was a common notebook computer and the software used for processing was MATLAB.

The reference video recording system was based on a commercial video camera (PowerShot G7, Canon) with an optical zoom lens with 25–210 mm focal length; the video format is National Television System Committee (NSTC) with frame rate of 30 frames (images) per second with 640 $\times$ 480 pixels per frame. The processing was performed on an ordinary computer (Latitude D830, Dell) with a MATLAB software package similar to the one in [12], giving a tracking accuracy of around 1 mm. Fig. 3(c) shows the video recording system.

For modeling tremor, we used a tremulous arm model similar to the one we used in [37]. It consisted of a conduction coil, an ac generator source, and a solid arm model with a small magnet attached. The ac generator produced a sinusoidal wave with a frequency range of 3–12 Hz and different amplitudes that reflected different disease severities. The generator was wired to a transformer and created a varying magnetic field in its core that induced a varying electromotive force. The force acted on the magnet attached to the solid arm model and generated a periodic movement of the arm at the ac generator frequency. The solid body is a plastic sheet filled with cardboard at the typical size of an arm (40 $\times$ 10 cm^2). We assumed that the arm model was rigid, i.e., the frequency of tremor was the same over its entire surface. This assumption is reasonable because of the relatively high rigidity of the plastic and the relatively small EM force. A 26-cm-long and 8-cm-wide metal sleeve made out of an aluminum foil was attached to the arm 10 cm from the arm base to simulate reflection from real arm. A small red LED marker was attached in the middle of the metal foil, at a distance of 23 cm from the body for the video reference system. Fig. 3(d) shows the tremulous arm model.

The arm model was built to have similarities to neurological disease tremors. First, the arm model displacements are in inverse proportion to the tremor frequency like TBPs of neurological disease patients [47]. Second, the arm model tremor has resonance frequency similar to the arms of PD patients [48]. In the arm model, the resonance frequency, which is determined by the arm dimensions and material, was around 5 Hz. Third, the tremor amplitudes of the arm model varied along the model length (the amplitude was higher closer to the hand) because the body restrains arm movement. Unlike the carton board that does not reflect most of the UWB radiation, a real body part that

Fig. 4. Three different interferers from left to right: two static metal reflectors, a wooden wall separating the arm model and the UWB sensor node prototype, and a person with aluminum foil sleeve moving his hand at a normal pace of 1 Hz in the background.

is composed also from water reflects sometimes a major part of its radiation [41]. To simulate the body part and the clothing and the cloth material reflection, a wrinkled metal strip was attached to the arm model.

The UWB acquisition system and the reference video system were placed in an orientation relative to the arm model that enabled measuring displacement in 1-D. The arm surface was moving to and from the UWB acquisition system, and horizontal to the video camera, to capture the full tremor amplitude. The UWB system antennas were placed in an optimal orientation to capture the maximum reflection from the arm model. The arm model was placed in a set of distances that moved between 1 and 2 m from the acquisition systems.

Two sets of experiments were performed. The first set was performed with varying distances of 1, 1.5, and 2 m between the arm and the acquisition system. For each distance, the tremulous arm model fluctuated at a single frequency from 3 to 12 Hz. The UWB and video recording systems were activated simultaneously and recorded data for 20 s.

The second set of experiments tested the robustness of the system to common interferers: a static metal reflectors; a wooden wall between the arm model and the sensor node; and a person moving his arm covered with a metal sleeve in the background at a frequency of approximately 1 Hz.

Each interferer simulated a different effect: the metal reflector induced static MPCs that were not related to the TBP; the wall simulated any surface that blocks part of the radiation; and a moving arm in the background induced MPCs with varying delays at a slower pace than the tremulous arm. The distance between the UWB system and the arm was fixed to 1.5 m, and the induced frequency was 5 Hz. Fig. 4 shows the system with the three different interferers.

V. Results and Discussion

A. UWB Tremor Acquisition System Results

1) Coarse Results: Fig. 5 shows the spatiogram (time-space representation) of the received signal as defined in (3) in a range of 10 cm around the arm location, calculated by multiplying the propagation delay by the speed of light. The arm model was at a distance of 1.5 m from the UWB system, and the tremor frequency was 5 Hz. The colors in the spatiogram represent the received signal amplitude in volts. The MPCs related to the arm can be detected in a range of 10–20 cm from the central location

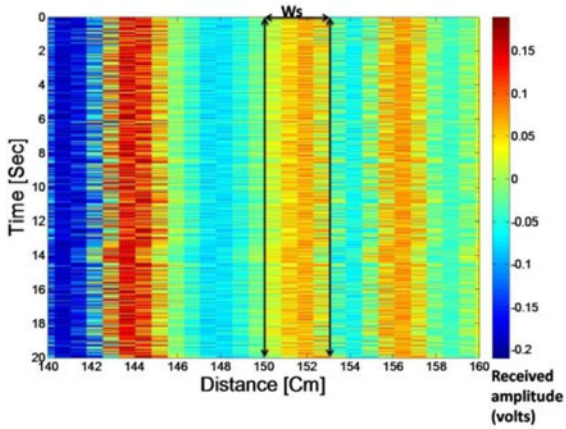

Fig. 5. Typical received signal in a time-space representation in an observation period of 20 s and region of 20 cm. The colors indicate the intensity of the received signal. The lines mark an area of the window used for tremor detection. Most of tremor fluctuations were captured inside the window of size that reflects the clinical tremor amplitude constraints. The red points represent the pick of the frequencies, which represents the frequency estimate of 5 Hz.

by the pattern of fluctuations in the spatiogram. The sliding window of $W_s = 3$ cm in (7) is applied in the figure at a distance of 150–153 cm from the acquisition system, capturing tremor amplitudes of up to 1.5 cm. For each sample, we calculated the time shifts by the CM according to (7). Then, we applied the temporal constraint by filtering according to (8), each of the delay waveforms with a bandpass filter (60 taps finite impulse response (FIR) filter, passband of 3–12 Hz and stop band of 2–15 Hz with design method FIR least-squares).

The selected fingers after applying the constraints were likely to contain MPCs related only to reflections from the arm. The estimated frequencies in this experiment are shown in Fig. 6. The frequency estimates were derived for each of the filtered time shift vectors according to (12). Most of the filtered time shifts fluctuated in frequency range of 5–10 Hz, which is similar to the induced frequency (5 Hz) and to its first harmonic (10 Hz). The histogram of the estimated amplitudes for the same experiment is shown in Fig. 7. It was derived for each of the filtered time shift vectors according to (13). The amplitudes varied between 0 and 1.2 cm, which was similar to the tremor amplitude constraint boundaries. The low-amplitude estimates in the histogram are related either to the areas where the arm movement is constrained by the body or to other static reflectors.

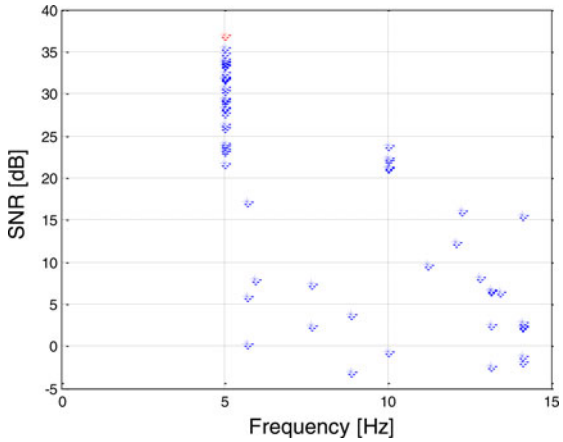

Fig. 6. UWB frequency estimations' histogram of MPCs related to the arm (after applying the constraints) for the arm with a 5 Hz tremor. The frequency is well detected with mean error from the ac generator reference of less than 0.1 Hz. The second signal harmonic can be detected at frequency of 10 Hz.

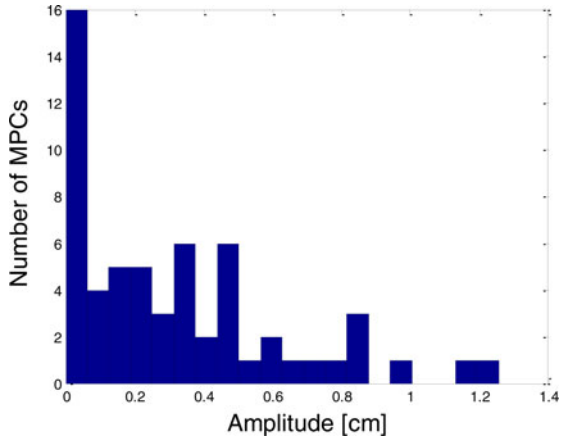

Fig. 7. UWB amplitude estimations' histogram of MPCs related to the arm (after applying the constraints) for the arm with a 5-Hz tremor. The set of amplitude estimates ranges between zero (small displacements, relating to the part of arm which is constrained by the body) and 1.2 cm (maximal displacements, relating to the part of arm near the hand).

The received SNR varied between 15 and 45 dB. The fingers of time shift vectors are chosen according to (10) with $\mathrm{SNR}_{\mathrm{TH}}$ equal to 0.8 of the maximal SNR value. The time shifts that relate to the TBP are combined according to the frequency content with weights according to (11). The tremor's frequency and the maximal amplitude are estimated according to (12) and (13).

The average tremor frequency estimation error, calculated in reference to the induced frequency from the ac signal generator, was around 0.01 Hz with standard deviation of less than 0.005 Hz. The excellent tremor frequency approximation accuracy is due to a single tremor frequency present in the experiment.

Fig. 8 shows the estimated maximal amplitude as a function of the induced tremor frequency for the different distances between the arm and the acquisition system. The approximated amplitude decreases with frequency as expected from the mechanical properties of the arm model. Near the frequency of 5 Hz, there is a peak which indicates the resonance frequency.

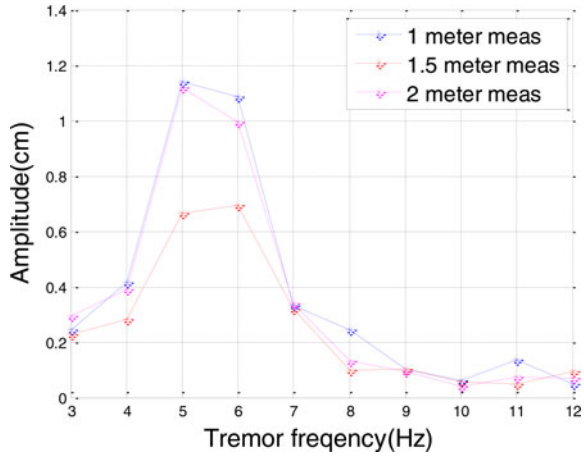

Fig. 8. UWB maximal amplitude approximations for the different distances after combining of the MPCs with the highest SNR (MRC combining). The tremor amplitude declines with tremor frequency but around 5 Hz, the resonance frequency, there is an increase in amplitude. The amplitude estimations are highly correlated (0.97) but can vary in magnitude as the SNR criterion can include lower tremor amplitudes from the inner part of the arm.

The amplitude estimations for the different arm positions were highly correlated with a correlation factor of 0.97. In this experiment, the amplitude estimation at a distance of 1.5 m was lower by 40% than the amplitudes estimation of the other distances. This difference can be explained by MPCs with relatively high SNRs that were reflected not from near the free-to-move hand but closer to the restraining body. Thus, the combining process included some fingers with low amplitudes. In the future, with a smaller sleeve, the TBP amplitude variability can be minimized.

The video system was used for each experiment as a reference for the UWB amplitude estimations. While the UWB sleeve is wide and includes many tremor displacements along its surface, the optical-based video system estimated displacement of a single point where the marker was attached. As a result, fair compartment of the UWB amplitude estimations to any single point acquisition method is difficult and might suffer from inaccuracies. Still, when the video marker is in some specific locations that can be used as prior knowledge by the MPC combining algorithm, e.g., in the center of the TBP, a coarse evaluation of the UWB amplitude estimation quality is enabled.

To compare the amplitude estimations of the UWB system with the one of the video system, we used the known geometrical properties of the arm model. Higher tremor amplitudes are more statistically distinguished in the UWB system and result in higher SNR. Thus, our finger selection criterion, based on maximum SNR, is biased to choose MPCs reflected near the hand which is relatively free to move and has higher amplitudes rather than MPCs reflected from areas near the restraining body. This comparison greatly depends on the accuracy of the assumption, but it gives a fair base for point to point comparison.

The UWB amplitude estimation for the video red LED marker position (23 cm from the body) can be estimated by multiplying the UWB amplitude estimation, related to the amplitude near the hand (36 cm from the body), by the geometrical ratio of 36/23. Fig. 9 shows the UWB and the video amplitude approximations

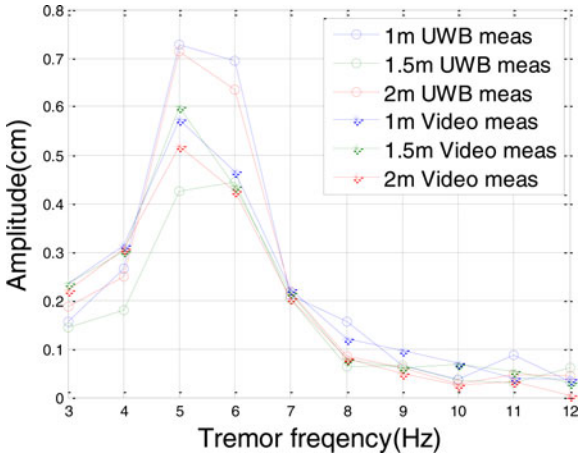

Fig. 9. UWB and video system amplitude estimation at a distance of 23 cm from the body after normalization. The average difference between UWB and video tremor amplitude estimations was 0.11 mm with standard deviation of 0.15 mm.

TABLE I
SYSTEM PERFORMANCE WITH DIFFERENT DISTURBERS

Disturbers Source	Received SNR (derived by FFT)	Frequency estimation error (Hz)	Amplitude estimation error (cm)
Metal reflector	36.99	0.0003	0.08
Wall	34.45	0.0005	-0.04
Human arm moving at 1 Hz pace	36.21	0.0006	-0.05
All disturbances together	37.05	0.0007	0.16

after normalization by the geometrical factor. The amplitude estimations of the two systems are highly correlated with a correlation factor of 0.95. The average amplitude estimation error of the UWB estimations compared to the reference video system was 0.16, 0.05, and 0.17 cm, with standard deviation of 0.23, 0.08, and 0.23 cm, and with maximal error of 0.61, 0.25, and 0.58 cm, for distances of 1, 1.5, and 2 m, respectively, between the UWB system and the arm.

2) System Tolerance to Different Interferers: A reference measurement without any disturbers was performed first for a distance of 1.5 m and induced frequency of 5 Hz. The frequency estimation was 4.999 Hz, the induced amplitude estimation was 0.44 cm, and the received SNR for the reference measurement was 36.18.

Measurements with all the interferers were then performed. The results are given in Table I. The received SNR for all measurements was above 34 dB which is sufficient to give the correct approximation. The frequency estimation error compared to the ac generator reference was excellent in all measurements, with a mean error from the ac generator source of less than 0.001 Hz. The metal reflector enhanced received SNR by 2.5% and the wall decreased the SNR by 5%. Still, as can be seen from the table, the amplitude estimations were accurate with absolute mean error of 0.08 cm and standard deviation of 0.1 cm from the video reference. The maximal amplitude error was 0.16 cm in the experiment with all disturbers.

This experiment showed that the detection algorithm we applied manages to filter out efficiently the interference of the different disturbers. As a result, the proposed UWB system seems to show tolerance to common interferers.

B. Comparison of the UWB Properties With the Common Tremor Acquisition Systems

1) General Technology Properties: Unlike the INS, the UWB and video systems are both based on exploiting EM wave reflection from the TBP of interest and thus share many similarities. The UWB system exploits reflection of UWB radiation (bandwidth of a few gigahertz) and the video system exploits reflection of white light (bandwidth of a few megahertz). Unlike the video system, the UWB system transmits EM radiation. Still, the average power is far lower than the radiation allowed by common radiation health and safety regulations.

The UWB system provides an integral set of amplitudes and frequencies over all the TBP area whereas the video and the INS systems provide punctual information. Furthermore, the UWB system provides information about all body parts and enables analysis of motion kinematics.

2) Working Volume: In an optical-based system, the coverage of the system is limited by the optical lens and by the dimensions of the room. The INS, as it is worn on the patient, is not limited to specific location. In an UWB system, since the UWB transmission can penetrate walls and other obstacles and the UWB radiation can propagate all over the environment, the patient mobility is not limited to a single room and to the area captured by camera lens.

3) Calibration: Video tracking systems require a calibration. A calibration phase is needed for relative displacement estimation and can be performed by utilizing an object with known dimensions. The INS requires offline calibration procedure for the gyroscope and accelerometers, which is sometimes tedious. In addition, due to phenomena like battery aging, an online calibration is needed to be performed. The UWB system does not require calibration. Still, a patient tracking procedure based on the UWB measurements should be applied in the beginning and during the system operation in order to improve system performance.

4) Wearablilty: The INS must be worn on patient for a period of days during daily life activities in which he needs to replace the sensor battery. The INS cannot be attached to any body part as wearing it can be inconvenient and furthermore it can slightly move along the body part during operation.

In most of the common optical systems a marker has to be attached to the body part of interest. Markerless techniques are not as accurate and their displacement estimation resolution decreases with the distance between the camera and the patient; they might not be able to detect efficiently small tremor amplitudes around 1 mm.

In the UWB system, in general, there is no need for a marker. A cloth, or a sleeve that is worn on the body part of interest, is enough to help distinguish between MPCs related to the body part and one that are not. Unlike the INS and optical systems, the cloth or the sleeve does not limit or restrict day life activities.

To simulate the reflection of the body part and the clothing effect and the cloth material reflection, a wrinkled metal strip was attached to the arm model. Even without any clothes or sleeve, with high enough pulse repetitions, the detection accuracy is not expected to be affected. With a low reflection coefficient of 25% (reflection decrease by up to a factor of 4, usually the reflection from body is assumed to be around 50%), with similar pulse repetition and transmission power level as in our experimental setup, this drop in the reflection will not affect the accuracy due to the high SNR tolerance in the system. (worst SNR range drop from 15 to 9 dB) is still sufficient SNR to detect the tremor efficiently.

5) Sensitivity: The optical system is sensitive to changes in light conditions and in marker orientation, to imperfect focus (the image of the light spot that represents the marker will go in and out of focus as the patient moves), and to other sources with similar illumination properties like the marker that can cause false detection, to inaccurate calibration.

The UWB and INS systems can work in any light condition including darkness. The INS is sensitive to inaccuracies in calibration, to battery drift, to sensor displacements.

The UWB is sensitive to movements in the medium having similar fluctuations in scale of few hertz. A precise tracking of patient location can help in filtering these fluctuations. Still, in non-line of sight (LOS) conditions where the MPCs are very spread, the task is more difficult.

6) Technology Estimation Accuracy: In all systems, the frequency estimation accuracy is high and the error is less than 0.1 Hz due to the repetitive nature of the tremor. The amplitude estimation accuracy is more sensitive in these systems.

The optical system accuracy moves from a fraction of millimeter to few centimeters depending on the video camera quality—the resolution of the frame, the number of frames per second, the calibration accuracy, the focus of the picture, the algorithms used, and more.

In the INS-based technologies, accuracy moves also from fraction of a millimeter to a few centimeters and depends on the sensors quality, the existence of a compass in addition to the accelerometer and gyroscope, the accuracy of calibration, the algorithms used, the place the sensor is attached, and more.

For the UWB system, it is important to emphasize that unlike the optical and the INS systems, it gives a set of frequencies and set of amplitudes from all over the TBP. Clinical evolution of the UWB system is a future work. From the experimental results in this paper, the accuracy can be around a milimeter, which is sufficient for most methods of tremor evaluation.

VI. Conclusion and Future Work

This paper describes a new noninvasive technology to monitor tremor and assess its parameters for diagnosis of different neurological pathologies. The UWB-based acquisition system has excellent frequency estimation with error less than 0.1 Hz and provides a set of tremor amplitudes along the TBP. The tremor frequency and the set of tremor amplitudes can be a base for an objective scale of tremor severity that can be used for medical diagnosis and help in verifying treatment affectivity.

The suggested UWB technology is still in development stages but promises to have many advantages over existing acquisition systems. One major advantage of the UWB acquisition system over the optical-based system and over INS is that it includes information of all TBPs and can gives additional information on patient kinematics, which in the future can be aggregated in the analysis to improve the quality of the medical diagnosis. Another advantage is that the UWB system can work with only a comfortable sleeve and does not require attaching inconvenient markers; it is not sensitive to light conditions and is not limited in space like the video system.

A lot of research is still needed to make this technology feasible for clinicians. In the future, multiple small size UWB sensor nodes with an approximate size of $10 \times 10\ \text{cm}^2$, operating with common standards (e.g., by 802.15.4a standard [37]), well synchronized, and placed in different locations in an indoor environment are expected to offer continuous noncontact 3-D tremor assessment from all body parts. The system can be extended to include also information about patient kinematics, e.g., statistics about rate of freezing, which is a common indicator for PD, and can be used to improve the reliability of the suggested disease score. The UWB data transmission capabilities can be further used to transfer the raw data from the sensor node to an UWB hub with internet access to enable long-term tremor monitoring.

This study is a pioneering work in the field of tremor assessment. It promises to give an objective accurate scale of tremor severity that can be obtained during daily life activities of the patient in convenient manner.

Acknowledgment

The authors would like to thank the anonymous reviewers for their very helpful comments and questions and for their feedback on the contribution of this work that was integrated in the paper.

References

[1] H. Ben-Pazi, H. Bergman, J. A. Goldberg, N. Giladi, D. Hansel, A. Reches, and E. S. Simon, "*Synchrony of rest tremor in multiple limbs in Parkinson disease: evidence for multiple oscillators*," *J. Neural Transmiss.*, vol. 108, pp. 287–296, 2001.

[2] P. Martínez-Martín, A. Gil-Nagel, L. M. Gracia, J. B. Gómez, J. Martínez-Sarriés, and F. Bermejo, "Unified Parkinson's disease rating scale characteristics and structure," *Movement Disorders*, vol. 9, pp. 76–83, 1994.

[3] C. Bor-Rong, S. Patel, T. Buckley, R. Rednic, D. J. McClure, L. Shih, D. Tarsy, M. Welsh, and P. Bonato, "A web-based system for home monitoring of patients with Parkinson's disease using wearable sensors," *IEEE Trans Biomed. Eng.*, vol. 58, no. 3, pp. 831–836, Mar. 2010.

[4] G. Grimaldi and M. Manto, "Neurological tremor: Sensors, signal processing and emerging applications," *Sensors*, vol. 10, pp. 1399–1422, 2010.

[5] R. C. Eberhart, "Tremor quantification using digital actigraphy," in *Proc. First Joint BMES/EMBS Conf.*, 1999, vol. 1, p. 521.

[6] J. Jankovic and J. D. Frost, Jr., "Quantitative assessment of parkinsonian and essential tremor: Clinical application of triaxial accelerometry," *Neurology*, vol. 31, pp. 1235–1240, Oct. 1981.

[7] A. Salarian, H. Russmann, C. Wider, P. R. Burkhard, F. J. G. Vingerhoets, and K. Aminian, "Quantification of tremor and bradykinesia in Parkinson's disease using a novel ambulatory monitoring system," *IEEE Trans. Biomed. Eng.*, vol. 54, no. 2, pp. 313–322, Feb. 2007.

[8] U. X. Tan, K. C. Veluvolu, L. Win Tun, S. Cheng Yap, C. N. Riviere, and A. Wei Tech, "Estimating displacement of periodic motion with inertial sensors," *IEEE Sens. J.*, vol. 8, no. 8, pp. 1385–1388, Aug. 2008.

[9] Y. K. Thong, M. S. Woolfson, J. A. Crowe, B. R. Hayes-Gill, and D. A. Jones, "Numerical double integration of acceleration measurements in noise," *Measurement*, vol. 36, pp. 73–92, 2004.
[10] C. B. Alan, *Handbook of Image and Video Processing*. San Diego, CA: Academic, 2005.
[11] R. D. Green and G. Ling, "Quantifying and recognizing human movement patterns from monocular video images—part II: Applications to biometrics," *IEEE Trans. Circuits Syst. Video Technol.*, vol. 14, no. 2, pp. 191–198, Feb. 2004.
[12] A. Jobbagy and G. Hamar, "PAM: Passive marker-based analyzer to test patients with neural diseases," in *Proc. 26th Annu. Int. Conf. IEEE Eng. Med. Biol. Soc.*, 2004, pp. 4751–4754.
[13] I. D. Peikon, N. A. Fitzsimmons, M. A. Lebedev, and M. A. L. Nicolelis, "Three-dimensional, automated, real-time video system for tracking limb motion in brain-machine interface studies," *J. Neurosci. Methods*, vol. 180, pp. 224–233, 2009.
[14] Z. Uhrikova, O. Sprdlik, V. Hlavac, and E. Ruzicka, "Action tremor analysis from ordinary video sequence," in *Proc. Annu. Int. Conf. IEEE Eng. Med. Biol. Soc.*, 2009, pp. 6123–6126.
[15] M. Ivan, "Electromyographic differentiation of tremors," *Clin. Neurophysiology: Official J. Int. Fed. Clin. Neurophysiol.*, vol. 112, pp. 1626–1632, 2001.
[16] M. R. Mahfouz, M. J. Kuhn, G. To, and A. E. Fathy, "Integration of UWB and wireless pressure mapping in surgical navigation," *IEEE Trans. Microw. Theory Tech.*, vol. 57, no. 10, pp. 2550–2564, Oct. 2009.
[17] T. A. C. Nizet, M. E. A. C. Broeders, and H. T. M. Folgering, "Tremor side effects of salbutamol, quantified by a laser pointer technique," *Respiratory Med.*, vol. 98, pp. 844–850, 2004.
[18] E. O. S. Padraig and B. D. Richard, Jr., "Validation for tremor quantification of an electromagnetic tracking device," *Movement Disorders*, vol. 16, pp. 265–271, 2001.
[19] Z. Uhríková, O. Sprdlík, M. Hoskovcová, A. Komárek, O. Ulmanová, V. Hlaváč, C. D. Nugent, and E. Růžička, "Validation of a new tool for automatic assessment of tremor frequency from video recordings," *J. Neurosci. Methods*, vol. 198, pp. 110–113, 2011.
[20] K. C. Veluvolu and W. T. Ang, "Estimation of physiological tremor from accelerometers for real-time applications," *Sensors*, vol. 11, pp. 3020–3036, 2011.
[21] A. Louis, "Sensor placement for activity detection using wearable accelerometers," in *Proc. Int. Conf. Body Sensor Netw.*, 2010, pp. 24–29.
[22] N. Kyriazis, I. Oikonomidis, and A. A. Argyros, "Efficient model-based 3d tracking of hand articulations using kinect," in *Proc. Brit. Mach. Vision Conf.*, 29 Aug. 29–Sep. 2,, 2011, pp. 1–11.
[23] S. S. Ram, Y. Li, A. Lin, and H. Ling, "Doppler-based detection and tracking of humans in indoor environments," *J. Franklin Inst.*, vol. 345, pp. 679–699, 2008.
[24] S. Z. Gurbtiz, W. L. Melvin, and D. B. Williams, "Comparison of radar-based human detection techniques," in *Proc. Conf. Rec. 41st Asilomar Conf. Signals, Syst. Comput.*, 2007, pp. 2199–2203.
[25] C. Hornsteiner and J. Detlefsen, "Characterisation of human gait using a continuous-wave radar at 24 GHz," *Adv. Radio Sci.*, vol. 6, pp. 67–70, 2008.
[26] J. M. Hausdorff, M. E. Cudkowicz, R. Firtion, J. Y. Wei, and A. L. Goldberger, "Gait variability and basal ganglia disorders: Stride-to-stride variations of gait cycle timing in Parkinson's disease and Huntington's disease," *Mov. Disord.*, vol. 13, pp. 428–437, 1998.
[27] F. E. Nathanson, J. P. Reilly, and M. N. Cohen, *Radar Design Principles: Signal Processing and the Environment, Second Edition*, 2nd ed. New York: SciTech, 1999, ch. 1.6.
[28] Y. Ruiqing, S. Redfield, and L. Huaping, "High-precision indoor UWB localization: Technical challenges and method," in *Proc. IEEE Int Conf. Ultra-Wideband*, 2010, pp. 1–4.
[29] IEEE 802.15 WPAN Low Rate Alternative PHY Task Group 4a (TG4a) [Online]. Available at http://www.ieee802.org/15/pub/TG4a.html
[30] Z. Jinyun, P. V. Orlik, Z. Sahinoglu, A. F. Molisch, and P. Kinney, "UWB systems for wireless sensor networks," *Proc. IEEE*, vol. 97, no. 2, pp. 313–331, Feb. 2009.
[31] I. Y. Immoreev, "Practical applications of UWB technology," *IEEE Aerosp. Electron. Syst. Mag.*, vol. 25, no. 2, pp. 36–42, Feb. 2010.
[32] C. Chang and A. Sahai, "Object tracking in a 2D UWB sensor network," in *Proc. Conf. Record 38th Asilomar Conf. Signals, Syst. Comput.*, 2004, vol. 1, pp. 1252–1256.
[33] X. Zhuge, T. G. Savelyev, A. G. Yarovoy, L. P. Ligthart, J. Matuzas, and B. Levitas, "Human body imaging by microwave UWB radar," in *Proc. Eur. Radar Conf.*, 2008, pp. 148–151.
[34] E. M. Staderini, "UWB radars in medicine," *IEEE Aerosp. Electron. Syst. Mag*, vol. 17, no. 1, pp. 13–18, Jan. 2002.
[35] B. Levitas, J. Matuzas, and M. Drozdov, "Detection and separation of several human beings behind the wall with UWB Radar," in *Proc. Int. Radar Symp.*, 2008, pp. 1–4.
[36] G. Blumrosen, M. Uziel, B. Rubinsky, and D. Porrat, "Non-contact UWB radar technology to assess tremor," in *Proc. 12th Mediterr. Conf. Med. Biol. Eng. Comput.*, May 27–30, 2010, pp. 490–493.
[37] G. Blumrosen, M. Uziel, B. Rubinsky, and D. Porrat, "Tremor acquisition system based on UWB Wireless Sensor Network," in *Proc. Body Sensor Netw. Conf.*, Jun.7–9, 2010, pp. 187–193.
[38] J. A. Gallego, E. Rocon, J. O. Roa, J. C. Moreno, A. D. Koutsou, and J. L. Pons, "On the use of inertial measurement units for real-time quantification of pathological tremor amplitude and frequency," *Procedia Chem.*, vol. 1, pp. 1219–1222, 2009.
[39] A. F. Molisch, J. R. Foerster, and M. Pendergrass, "Channel models for ultrawideband personal area networks," *IEEE Wireless Commun.*, vol. 10, no. 6, pp. 14–21, Dec. 2003.
[40] A. G. Yarovoy, L. P. Ligthart, J. Matuzas, and B. Levitas, "UWB radar for human being detection," *IEEE Aerosp. Electron. Syst. Mag.*, vol. 23, no. 5, pp. 36–40, May 2008.
[41] C. G. Bilich, "Bio-medical sensing using ultra wideband communications and radar technology: A feasibility study," in *Proc. Pervasive Health Conf. Workshops*, 2006, pp. 1–9.
[42] S. Gezici, C. Mung, H. V. Poor, and H. Kobayashi, "Optimal and suboptimal finger selection algorithms for MMSE RAKE receivers in impulse radio ultra-wideband systems," in *Proc. IEEE Wireless Commun. Netw. Conf.*, 2005, vol. 2, pp. 861–866.
[43] N. Boubaker and K. B. Letaief, "A low complexity MMSE-RAKE receiver in a realistic UWB channel and in the presence of NBI," in *Proc. Wireless Commun. Netw. Conf.*, 2003, vol. 1, pp. 233–237.
[44] M. Avriel, *Nonlinear Programming: Analysis and Methods*. New York: Dover, 2003.
[45] C. J. Jacobus and R. T. Chien, "Two new edge detectors," *IEEE Trans. Pattern Anal. Mach. Intell.*, vol. PAMI-3, no. 5, pp. 581–592, Sep. 1981.
[46] J. G. Proakis, *Digital Communications*, 3rd ed. New York: McGraw-Hill, 1995, pp. 780–782.
[47] R. J. Elble, S. L. Pullman, J. Y. Matsumoto, J. Raethjen, G. Deuschl, and R. Tintner, "Tremor amplitude is logarithmically related to 4- and 5-point tremor rating scales," *Brain*, vol. 129, pp. 2660–2666, Oct. 2006.
[48] J. J. Jankovic and E. Tolosa, "Parkinson's disease and movement disorders," *Eur. J. Neurol.*, vol. 10, pp. 603–604, 2003.

Gaddi Blumrosen was born in Jerusalem, Israel. He received the B.Sc. degree in electrical engineering from the Technion—Israeli Institute of Technology, Haifa, Israel, the M.S. degree in electrical engineering from Tel Aviv University, Tel Aviv, Israel, and the Ph.D. degree in biomedical engineering from the Hebrew University of Jerusalem, Jerusalem, Israel, in 2011.

He was involved in various research and development positions in the field of wireless communication and signal processing. He is currently a Valachi Pikovsky Foundation Postdoctoral Fellow at Tel Aviv University. His current research interests include wireless communication, radar and sonar systems, tracking systems, and biomedical signal modeling and processing.

Moshe Uziel was born in Jerusalem, Israel. He received the B.E. degree in physics, and the M.S. degree in applied physics, both from the Hebrew University of Jerusalem, Jerusalem, Israel, in 2008 and 2010, respectively.

He is currently an Engineer with Insightec Ltd., Tirat Carmel, Israel. His current research interests include radar and sonar systems and tracking.

Boris Rubinsky received the B.Sc. and M.Sc. degrees from the Technion—Israeli Institute of Technology, Haifa, Israel, and the Ph.D. degree in mechanical/bioengineering from the Massachusetts Institute of Technology, Cambridge, MA.

He is currently a Professor of the Graduate School at the University of California at Berkeley, Berkeley. His research is in the field of biomedical device technology. Highlights of his scientific contributions published in close to 300 peer review publications include conceiving and first clinical implementation in cryosurgery of the concept of real-time imaging monitored minimally invasive surgery, developing the first microelectroporation chip for cellomics and inventing and clinical implementation of nonthermal irreversible electroporation.

Dana Porrat received the Ph.D. degree in electrical engineering from Stanford University, Stanford, CA, in 2003.

She was a Postdoctoral Researcher at the University of California at Berkeley and in the Technion—Israeli Institute of Technology. She joined the School of Engineering, Hebrew University of Jerusalem, Jerusalem, Israel, in 2005. She investigates wideband radio communication systems and focuses on two fundamental aspects. In her laboratory, she measures physical properties of radio propagation in buildings in order to statistically characterize channel stability as terminals move. She is also interested in information theoretical analysis that offers powerful means in connecting models of radio channels to their inherent limitations in terms of the data rate of communication systems.